Nanoscale

Accepted Manuscript

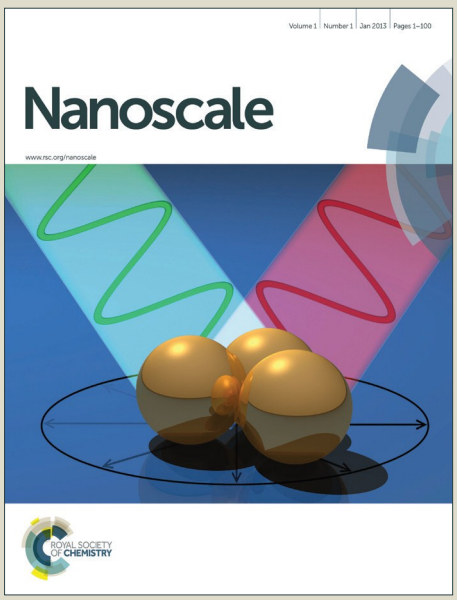

ROYAL SOCIETY OF CHEMISTRY

www.rsc.org/nanoscale

Nanoscale

ARTICLE

A One-step Approach to the Large-scale Synthesis of Functionalized MoS_2 Nanosheets by Ionic Liquid Assisted Grinding

Received 00th January 20xx,
Accepted 00th January 20xx

DOI: 10.1039/x0xx00000x

www.rsc.org/

Wentao Zhang, Yanru Wang, Daohong Zhang, Shaoxuan Yu, Wenxin Zhu, Jing Wang, Fangqing Zheng, Shuaixing Wang and Jianlong Wang*

A prerequisite for exploiting most proposed applications for MoS_2 is the availability of water-dispersible functionalized MoS_2 nanosheets in large quantities. Here we report one-step synthesis and surface functionalization of MoS_2 nanosheets by a facile ionic liquid assisted grinding method with the presence of chitosan. The selected ionic liquid with suitable surface energy could efficiently overcome the van der Waals force between the MoS_2 layers. Meanwhile, chitosan molecules bind to the plane of MoS_2 sheets noncovalently, which prevents the reassembling of exfoliated MoS_2 sheets and facilitates the exfoliation progress. The obtained chitosan functionalized MoS_2 nanosheets possess favorable stability and biocompatibility, which renders them as promising and biocompatible near-infrared agent for photothermal ablation of cancer. This contribution provides a facile way for the green, one-step and large-scale synthesis of advanced functional MoS_2 materials.

Introduction

Transition-metal dichalcogenides materials have garnered increased attention and have been intensely studied recently due to their unique structural, mechanical, electronic and optical properties, which originate from low dimensionality. As the most prominent example of these emerging materials, molybdenum disulfide (MoS_2) has received a fair share of attention in areas ranging from energy and catalysis to sensing.[1-4] Particularly, with higher absorbance in the near-infrared (NIR) region than that of both graphene and gold nanorods, MoS_2 nanosheets have been wildly applied as an efficient photothermal agent for the photothermal therapy (PTT) of cancers. Moreover, with high specific surface areas and hydrophobic plane, MoS_2 nanosheets can highly efficiently deliver therapeutic molecules for the combined therapy of cancer, such as combined photothermal and chemotherapy, combined photothermal and photodynamic therapy, and imaging guided photothermal therapy.[5-7]

However, the exploitation of most proposed applications of MoS_2 has been hampered by the lack of a simple method for the availability of MoS_2 sheets in large quantities. In principle, the layered MoS_2 crystal is composed of hexagonal layers of Mo atoms sandwiched between two layers of S atoms covalently, arranged as three planes of atoms (S-Mo-S). Similar to graphite, the loosely stacking of adjacent sheets via van der Waals interactions enables the formation of bulk crystal. Fortunately, the weak van der Waals forces between the layers are prone to be broken, dividing bulks into the layered compounds, and this controllable exfoliation is an exclusive way to obtain mono- or few-layered MoS_2 through externally applied forces.[8, 9] To date, abundant efforts have been paid to the exfoliation of MoS_2 into individual layers, including micromechanical cleavage or the so-called "Scotch tape method", intercalation-driven exfoliation, liquid-phase sonication exfoliation or grinding assisted liquid phase exfoliation, laser or plasma etching and electrochemical exfoliation. Of all these methods, the adhesive tape procedure, performed in most of the fundamental studies on the properties of the single and few layer MoS_2, however, is clearly not compatible with large-scale synthesis for practical applications.[10] It has been known for many years that intercalation-driven exfoliation based on the intercalation of lithium ions (Li^+) in the interlayer space of the bulk material can exfoliate layered MoS_2. However, due to structural deformation, this chemical exfoliation method results in the loss of the MoS_2 nanosheets' semiconducting properties and quenching of photoluminescence in 2D MoS_2.[11] Additionally, the lithium intercalation method is time-consuming, extremely sensitive to environment and not safe in laboratory.[12] A major breakthrough was made by the exfoliation of layered MoS_2 materials in various organic solvents via sonication to generate mono- or multilayer structures, which was initially proposed by Coleman co-workers in 2011 and then evolved by many scientists successively.[13, 14] However, these procedures are incompatible with most solvents and require harsh solvents or expensive equipment with extremely time-consuming multiple steps, leading to environmentally unfriendly, unsustainable and defect-rich practices. Very recently, unconventional exfoliation

College of Food Science and Engineering, Northwest A&F University, Yangling, 712100, Shaanxi, P. R. China. E-mail: wanglong79@yahoo.com
Electronic Supplementary Information (ESI) available: [the storage stability, quantification, extinction coefficient, and photothermal stability of CS-MoS_2, and contrast experiment]. See DOI: 10.1039/x0xx00000x

methods with sophisticated equipment and extremely low yield by laser or plasma etching and electrochemistry also have been initiated.[15-17] Consequently, the development of exfoliation method to obtain large amount of MoS_2 nanosheets remains to be solved before practical use can be realized.

In this contribution, we report a one-step, large-scale, facile, safe, low-cost, environmentally friendly method, namely ionic liquid (IL) assisted grinding, to obtain individual nanosheets from the bulk MoS_2. Ionic liquid is chosen owing to their unique properties, such as nonvolatile, non-flammability, low vapor pressure, and good electrical conductivity, which has emerged as a promising medium over the past decades in the area of synthesis, separation and electrochemistry.[18-23] Specially, researchers have demonstrated the debundling of single-walled carbon nanotubes (SWNTs) and functionalized ones with presence of IL. [20, 22] Most importantly, the exfoliation of graphene nanosheets and nanodots based on IL assisted grinding has been firstly reported by Shang and co-workers.[23] Being inspired by the debundling of SWNTs and graphene with IL, exfoliation by IL assisted grinding method is initiated as a new approach to synthetize MoS_2 nanosheets, which has never been explored before. Our procedure occurs at room temperature equipping only a mortar and pestle to mix the reactants and provide mechanical shear forces for the exfoliation of the MoS_2 sheets from bulk MoS_2. Nevertheless, to fully harness the capabilities of MoS_2 nanosheets, principally limited by its poor dispersity and stability in aqueous solutions, chitosan (CS) is introduced during the grinding process. The result product was then characterized and employed as a photothermal agent for the photothermal ablation of cancer in *vitro*.

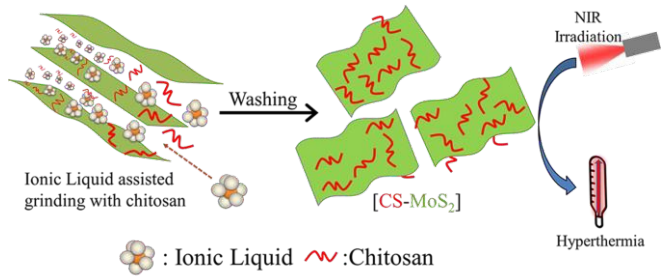

Scheme 1. Schematic to illustrate the facile exfoliation of MoS_2 by IL assisted grinding with the presence of chitosan, forming CS-MoS_2 nanosheets, which can sever as a photothermal agent.

Results and discussion

A one-step approach was employed to the large-scale synthesis of functionalized MoS_2 nanosheets by ionic liquid assisted grinding, as shown in Scheme 1. More details on the synthesis procedure can be found in the Experimental Section. In general for the solvent assisted exfoliation of the layered materials, the well matched surface energy of solvents and layered material could result in the minimized enthalpy of exfoliation and effective exfoliation of layered materials.[13, 23-27] According to a previous study, the surface energy of a solvent (γ) can be converted to surface tension (Γ) by equation $\gamma = \Gamma + TS_S$, where S_S is the surface entropy and the value of TS_S is ~29 mJ/m^2 for almost all liquids at room temperature.[27] Thus, the surface tension (~40 mN/m) of used IL could be converted to 69 mJ/m^2 the surface energy, which proper matches with literature values of the MoS_2 surface energy (that is ~75 mJ/m^2).[27-29] Consequently, the used IL can effectively overcome the inherent van der Waals forces between MoS_2 sheets, much in the same way as the debundling of graphene and SWNTs in IL, promoting the exfoliation of the individual MoS_2 sheets and preventing the detached MoS_2 layers from restacking. However, owing to their hydrophobic nature, the direct dispersion of native MoS_2 sheets in water has been generally considered unattainable.[6, 30-32] Thus, during the grinding process, chitosan was introduced alternatively to facilitate the physiological stability and biocompatibility of MoS_2 nanosheets.[5, 33] After removing organic residues and incompletely delaminated MoS_2 by centrifugation, a homogeneous and dark green dispersion of CS-MoS_2 nanosheets was obtained. To investigate the stability of the as-prepared CS-MoS_2 nanosheets, we monitored the UV-vis absorbance at 610 nm of the CS-MoS_2 dispersion for two weeks (Fig. S1). The colloidal suspension showed feeble absorbance decay even stood for 14 days, implying excellent colloidal stability in water. More excitingly, our CS-MoS_2 nanosheets showed no sign of aggregation and precipitation in water, buffer solution and even in cell medium, indicating well physiological stability of CS-MoS_2 nanosheets (Fig. 1a). The favorable physiological and storage stability of CS-MoS_2 sheets occurs due to the existence of chitosan molecules bound to the exfoliated sheets, inducing the truly homogeneous codispersion of CS and MoS_2 sheets and avoiding the aggregation of sheets caused by van der Waals interactions and hydrophobic interactions.[6, 34] The concentration of MoS_2 nanosheets was then determined to be 426.1 μg/mL by atomic absorption spectrum (AAS, Fig. S2), indicating our procedure is large-scale and high-yield (~17 *wt.*%).[24, 35]

To confirm the combination of CS and MoS_2 sheets, Fourier Transform Infrared spectroscopy (FT-IR) and Thermogravimetric analysis (TGA) experiments were conducted. FT-IR spectra of MoS_2, chitosan and our product were performed between 4000 and 400 cm^{-1}. As shown in Fig. 1b, CS-MoS_2 nanosheets produced very similar absorptions of native chitosan. The peaks at 1600 and 1410 cm^{-1} are assigned to the -NH and -CH_2 bending, respectively. CH_3 and C–O wagging are located at 1380 and 1340 cm^{-1}, respectively, while 1000 cm^{-1} is resulted from skeletal vibrations of O-C-C stretching.[33, 36] Moreover, the band at about 468 cm^{-1} presented in both case of MoS_2 and CS-MoS_2 is corresponded to Mo-S vibration.[37] The results indicate the coexistence of CS and MoS_2, meaning the formation of CS-MoS_2 complex. To better demonstrate the combination, TGA measurements under N_2 atmosphere at a heating rate of 10 ℃ min^{-1} were employed. As shown in Fig. 1c, negligible weight loss can be observed during the heating process from room temperature to 600 ℃ for native MoS_2. Two weight losses are observed in the TGA curve of CS. The weight loss before 150 ℃ is due to the moisture vaporization, while the weight loss over 220 ℃ is attributed

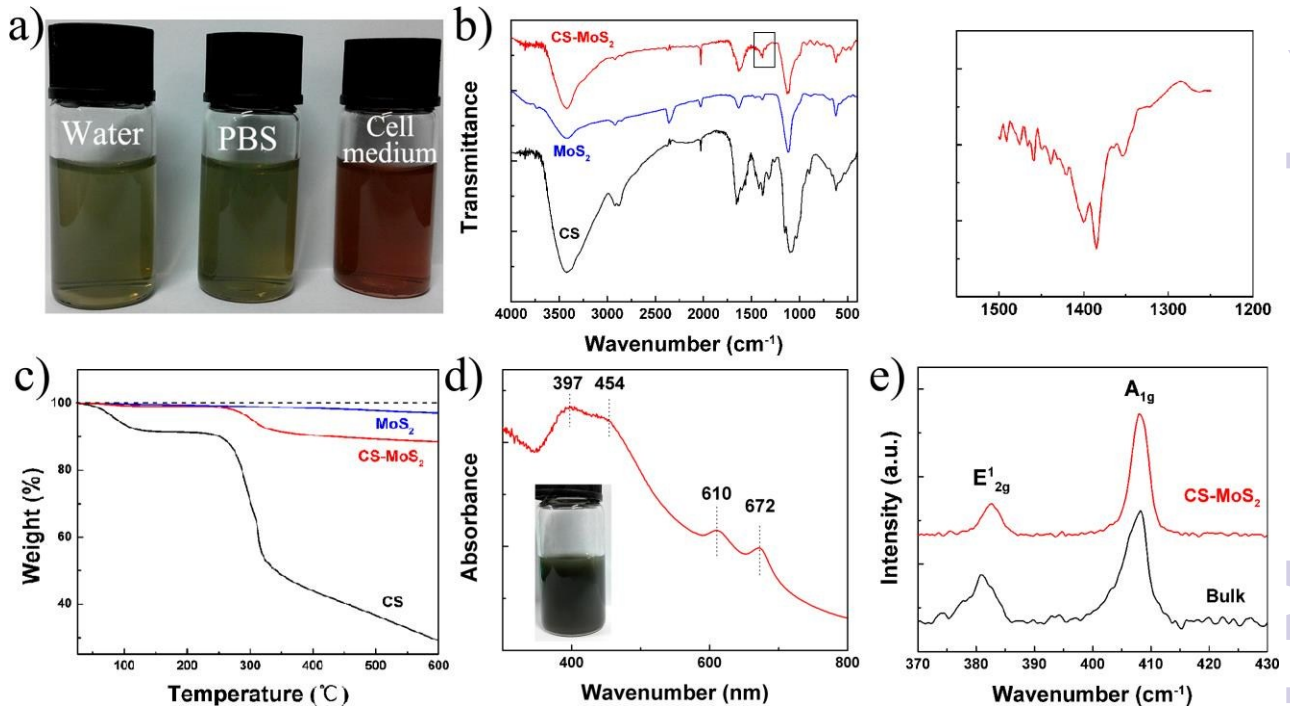

Fig. 1 Characterization of CS-MoS_2 nanosheets. (a) Photos of CS-MoS_2 nanosheets in water, PBS and cell medium, respectively. (b) FT-IR spectra for chitosan, native MoS_2 and CS-MoS_2 nanosheets, and enlarged FT-IR spectrum of CS-MoS_2 nanosheets in the range of 1250–1500 cm^{-1}. (c) TGA-mass loss curves of chitosan, native MoS_2 and CS-MoS_2 nanosheets. (d) UV-vis spectrum of CS-MoS_2 nanosheets, (Inset) a photo of CS-MoS_2 dispersion in water. (e) Raman spectra of natural MoS_2 and CS-MoS_2 nanosheets.

the degradation of CS molecules. Most prominently, once complex with CS, TGA of the intercalation compound reveals two decomposition onsets and a significant weight loss over 220 ℃, which agrees well with that of pure CS. The results of FT-IR and TGA adequately manifest the interaction between CS and MoS_2. Moreover, from the result of TGA experiments, the content of CS in our CS-MoS_2 nanosheets was calculated to be *ca.* 12.5 *wt.*%, which is obviously higher than that of previous report, namely ~5 *wt.*%.[5] The higher content of CS endows CS-MoS_2 nanosheets with better storage stability, superior biocompatibility and broader potential in many fields.[33, 36, 38]

With the certitude of successful interaction between CS and MoS_2, further characterizations were then conducted. Firstly, the optical absorption spectrum for our CS-MoS_2 suspension was measured using a UV-vis spectrometer with 1 nm steps (Fig. 1d). Typical characteristic absorption bands of MoS_2 located at 672, 610, 454 and 397 nm are observed, which are in good agreement with few-layered 2H-MoS_2 obtained from a liquid-based exfoliation method.[13, 25] The absorption peaks at 672 and 610 nm can be assigned to the direct excitonic transitions at the K point with the energy difference arising due to spin−orbital splitting of the valence band. Peaks at 454 and 397 nm correspond to the direct excitonic transitions of M point between higher density of state regions of the band structure.[25] According to the above results of UV-vis spectra and AAS, the extinction coefficient of the as-prepared MoS_2 was determined to be 62.6 L g^{-1} cm^{-1} (Fig. S3), which is higher than that of the chemically exfoliated MoS_2.[2, 6, 39] The result is reasonable a chemically exfoliated MoS_2 with the intercalation of Li^+ ion o the lamella of MoS_2, forming Li_xMoS_2, aggrandizes the relativ molar mass of MoS_2, which in turn leads to the imprecis calculation of extinction coefficient.[11] Importantly, with mil grinding process only relied on shear forces to exfoliate th MoS_2 layers from the bulk materials, the formation of sever defect on the crystalline plane is avoided. Thus, fewer defects generated during our synthesis process, compared to chemical exfoliation, might also contributed to higher extinction coefficient.[2] The result indicates that our IL assisted grinding exfoliation process induces less defects, resulting i high quality MoS_2 sheets.

The structural changes in the MoS_2 before and after exfoliation were elucidated by Raman spectroscopy at roo temperature and the spectra are shown in Fig. 1e. Raman spectra of both samples show two prominent peak corresponding to the in-plane E^1_{2g} and out-of-plane A_{1g} vibrations of MoS_2. Upon exfoliation of the bulk material t single and few layered MoS_2, the Raman peaks of E^1_{2g} red shifts to 382.7 cm^{-1} and A_{1g} shows a small blue shift, with th position difference (Δ) decreases from 27.3 of bulk to 25.3 cm^{-} further confirming the exfoliation of MoS_2. However, the ga between E^1_{2g} and A_{1g} peaks of our exfoliated CS-MoS_2 somewhat broadening when compared to those of th mechanically exfoliated MoS_2 layers.[2, 25] This might be due t the larger thicknesses of MoS_2 nanosheets caused by presence of CS on the surfaces. The typical morphologi

structures, and dispersivity of the CS-MoS_2 nanosheets were then analyzed by transmission electron microscopy (TEM) and scanning electron microscopy (SEM). In Fig. 2a, 2b and 2c, it is shown that CS-MoS_2 nanosheets have a well-defined laminar morphology with a uniform size of around 120 nm (Fig. 2d), wrinkled sheets and high dispersivity rather than large-size aggregated bulks, which are consistent with what is usually observed for exfoliated layered compounds.[13, 25] As the foremost method allowing definitive measurement of the thickness of layer crystals currently, atomic force microscopy (AFM) was then conducted to unambiguously verify the thickness of exfoliated sheets. The AFM results shown in Fig. 2e and 2f clearly reveal that CS-MoS_2 nanosheets have uniform shapes with a typical thickness of *ca.* 1.4 nm and undergo about a 0.5 nm increase versus pure single-layer MoS_2 nanosheets (*ca.* 0.9 nm), mainly attributable to the attachment of CS on both planes of the MoS_2 sheets. [5, 40]

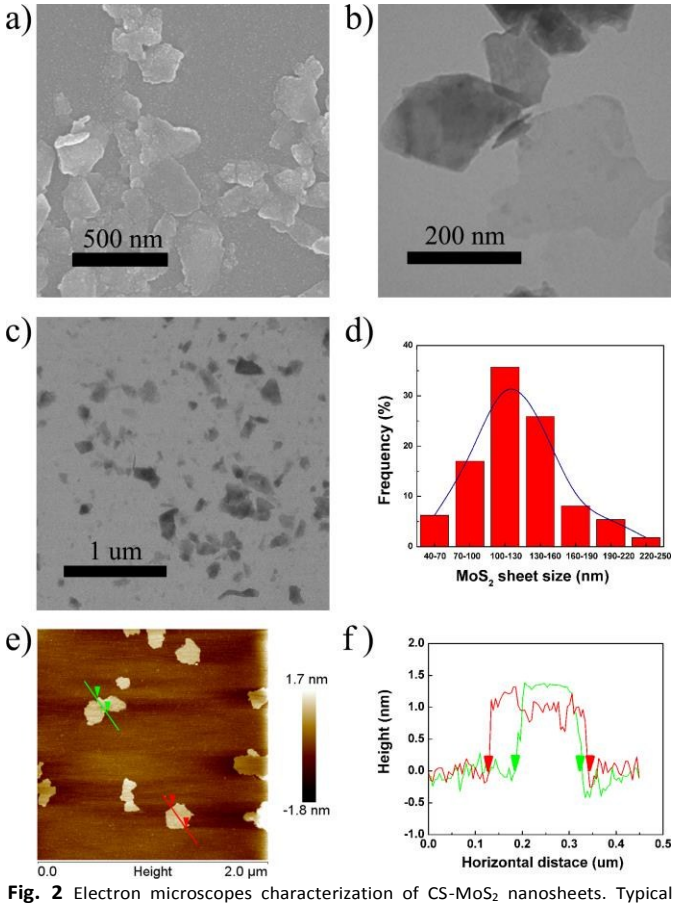

Fig. 2 Electron microscopes characterization of CS-MoS_2 nanosheets. Typical SEM (a), TEM (b and c) images of CS-MoS_2 nanosheets. (d) TEM measured size distribution of CS-MoS_2 nanosheets, over 100 sheets were counted. AFM image (e) and height profile across the CS-MoS_2 nanosheets in panel (f).

Additionally, the following three control experiments were also conducted: grinding with IL only, grinding in water or ethanol with chitosan. In all these cases, as expected, the obtained MoS_2 nanosheets dispersed in water aggregate significantly after standing for only 2 hours, shown in Fig. S4. Therefore, the co-grinding of chitosan and bulk MoS_2 in IL is the crucial point of the successful functionalization of individual MoS_2.

In view of above results, we have successfully proposed a new strategy for the large-scale fabrication of stable and functionalized MoS_2 nanosheets by ionic liquid assisted grinding. Although Yin and coworkers have reported an oleum based method to high-throughput synthesize CS-MoS_2, this approach requires harsh solvents and extremely time-consuming multiple steps.[5] By contrast, our facile strategy based on ionic liquid assisted grinding has several advantages: 1) with one-step approach to exfoliate and functionalize MoS_2 by grinding process, no expensive equipment with extremely time-consuming multiple steps was required, which seems to be more facile and convenient, 2) the reaction medium is ionic liquid, a recyclable and green organic solvent, thus with no environmental pollution, 3) the obtained CS-MoS_2 has higher content of CS, which might endow our CS-MoS_2 nanosheets with better storage stability and superior biocompatibility. These advantages allow this proposed synthetic approach to pave the way for the synthesis of advanced functional MoS_2 materials and extensive applications in nanomedicines.

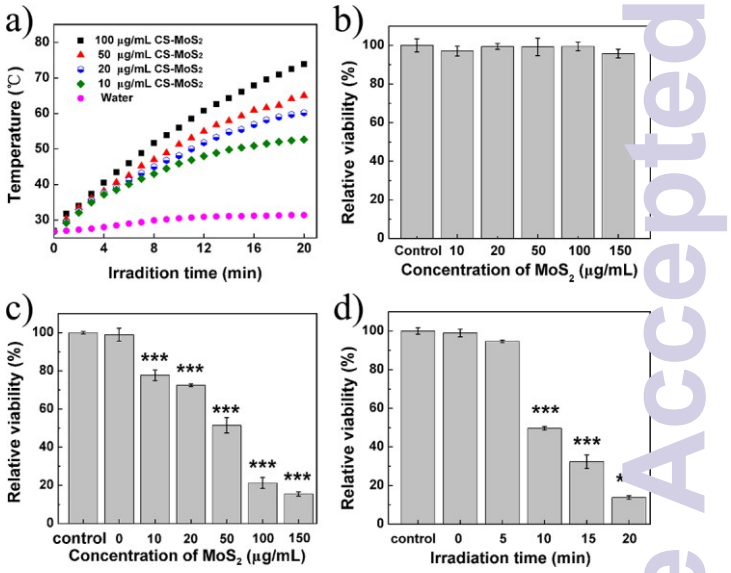

Fig. 3 Photothermal and biological activity of CS-MoS_2 nanosheets. (a) Photothermal heating curves of pure water and various concentrations of CS-MoS_2 nanosheets irradiated by 808 nm laser at power density of 2 W/cm^2 for 20 min. Relative cell viability data of HepG2 cells after incubation with CS-MoS_2 nanosheets at different concentrations for 24 h and then treated without (b) or with (c) 808 nm NIR irradiation for 10 min. (d) Relative cell viability after incubation with 50 μg/mL CS-MoS_2 nanosheets for 24 h and then treated with 808 nm NIR irradiation for various times. Results of cell viability are shown as the means ± SD of six separate experiments. *** < 0.001 versus control.

With superior performance, MoS_2 nanosheets and chitosan functionalized nanomaterials have been widely applied in nanomedicine.[5, 33, 39, 41] Herein, to verify our CS-MoS_2 nanosheets processing inherent properties of MoS_2 and CS, the photothermal heating and in *vitro* cytotoxicity experiments were conducted. The high molar extinction coefficient of CS-MoS_2 nanosheets in the NIR region, calculated to be 62.6 L g^{-1} cm^{-1}, indicated the potential of CS-MoS_2 nanosheets as

photothermal agent to efficiently convert NIR light into heat. To assess the light-to-heat conversion capability of aqueous dispersions containing different concentrations of the as-prepared CS-MoS_2 nanosheets (0–150 μg/mL), the solution temperature increased by NIR laser irradiation (808 nm, 2 W/cm^2) was recorded. Fig. 3a shows the temperature of the dispersions as a function of irradiation time. The blank test without CS-MoS_2 nanosheets shows negligible increase of temperature by less than 5 ℃. However, when irradiated with the presence of CS-MoS_2 nanosheets, the temperature of solution increased with the increasing concentration of CS-MoS_2 and irradiation time; the heating rate slower with extension of irradiation time, apparently as a result of faster heat loss at higher temperature.[42] At a concentration of CS-MoS_2 nanosheets above 10 μg/mL, the temperature of CS-MoS_2 dispersion induced by NIR irradiation for 10 min is higher than 43 ℃, which was considered to be high enough for PTT therapy of cancer.[41] Excitingly, our CS-MoS_2 nanosheets exhibited great photothermal stability without any significant decrease in the UV-vis absorbance even after exposure under laser for a certain period of time (Fig. S5), in marked contrast to gold nanorods, which are currently the subject of great interest for PTT but melted after being irradiated by the laser as reported in the literature.[43] These results indicate the capacity of our CS-MoS_2 nanosheets as a stable photothermal agent to convert the 808 nm laser energy into thermal energy for PTT.

Moreover, the abundant of biocompatible chitosan on the plane of MoS_2 nanosheets was expected to reduce the toxicity of MoS_2. To prove this, before we move on to further PTT experiments, the intrinsic toxicity of CS-MoS_2 nanosheets was studied by MTT assay with HepG2 cells. From Fig. 3b, it is apparent that, no significant differences in the cell viability were observed in the absence or presence of (5–150 μg/mL) CS-MoS_2 nanosheets. More importantly, the cellular viability was estimated to be greater than 95% after incubation with CS-MoS_2 nanosheets for 24 h even at a concentration of 150 μg/mL. These data show that our chitosan coated MoS_2 nanosheets have lower cytotoxicity compared to native MoS_2 or Li_xMoS_2, which might attributes to the abundant interspersion of biocompatible chitosan on the plane of MoS_2 sheets.[5, 44, 45]

With potent photothermal effect and excellent biocompatibility, the in *vitro* PTT therapy capacity of our CS-MoS_2 nanosheets was then evaluated. After incubation with 50 μg/mL CS-MoS_2 nanosheets for 24 hours in 24-well plates, HepG2 cells are exposed to an 808 nm laser irradiation for various time periods to evaluate the localized tumor photothermal effect of CS-MoS_2 nanosheets. To test their photothermal stability under an optical microscope, the irradiated cells are then stained with trypan blue. Fig. 4 shows images of samples irradiated for different time. As can be seen, cell death is shown as a blue spot and the proportion of dead cells increases with the extension of NIR laser irradiation time. By increasing the irradiation time to 15 min, the majority of the cancer cells were dead. The accordant results were then obtained by MTT test (Fig. 3d). After replanting the cells in a 96-well plate (n = 6) and incubation with or without 50 μg/mL CS-MoS_2 nanosheets, we monitored cell viability 24 h via MTT method after the photothermal treatment. The samples without irradiation by NIR laser showed no considerable dead cells, which also indicates our CS-MoS_2 nanosheets has good biocompatibility, while the viability of cells decreased dramatically with the extension of irradiation time and only about 13.82% of HepG2 cells remained viable after irradiation for 20 min. To further understand the PTT activity of CS-MoS_2 nanosheets, cytotoxicity experiments induced by NIR laser with different concentrations of CS-MoS_2 nanosheets were carried out. The cells were incubated with increasing amounts of CS-MoS_2 nanosheets (10, 20, 50, 100, 150 μg/mL) for 24 h and then irradiated with an 808 nm NIR laser for 10 min under a power density of 2 W/cm^2. Upon laser irradiation, cell viability noticeably decreased with the increasing concentration, and less than 16% of the cells remained alive after irradiation for 10 min (Fig. 3c). In accordance with the excellent photothermal responsiveness, MoS_2 nanosheets in our experiments can efficiently kill cancer cells by hyperthermia. These preliminary *in vitro* results confirm our expectations that our CS-MoS_2 nanosheets possessing excellent photothermal property for nanomedicine are comparable to MoS_2 nanosheets reported elsewhere.

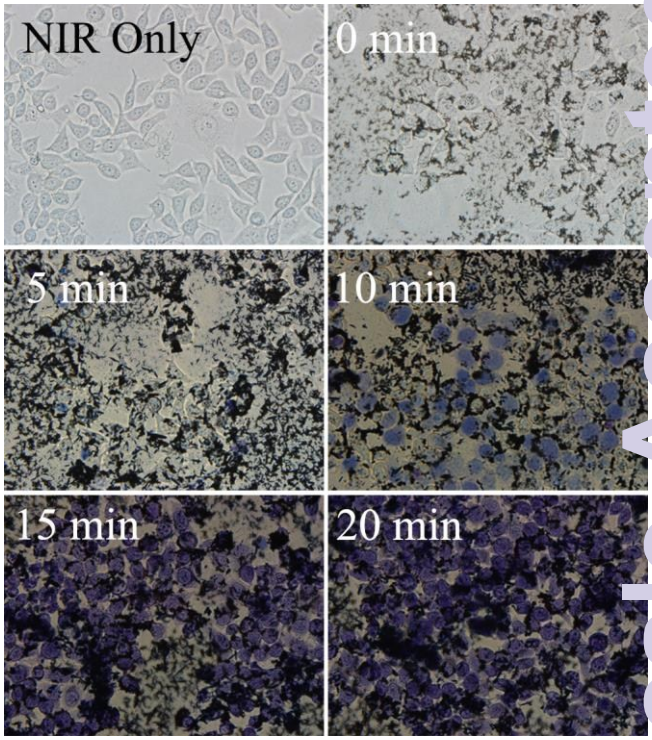

Fig. 4 Optical images of photothermal destruction of HepG2 cancer cells incubated with 50 μg/mL CS-MoS_2 nanosheets at various times of 808 nm NIR irradiation with power density of 2 W/cm^2. As can be stained by trypan blue, the dead cell emerges as a blue spot.

Experimental

Chemicals and Materials

Molybdenum (IV) sulfide (MoS_2) with a bulk particle size < 2 μm, 1-Butyl-3-methylimidazolium hexafluorophosphate

($BMIPF_6$) (≥ 97.0%), the IL used in this work, and CS were purchased from Sigma Aldrich. N,N-dimethylformamide (DMF), acetone and acetic acid, used during the washing process, were obtained from Sinopharm Chemical Reagent Co., Ltd.. 3-(4, 5-dimethylthiazol-2-yl)-2, 5-diphenyltetrazolium bromide (MTT) and trypan blue were purchased from MP Biomedicals LLC. All chemicals were used as received without any further purification. Deionized water was used in all experiments.

Synthesis of CS-MoS_2 nanosheets

Typically, using an agate mortar with a pestle, 250 milligrams of bulk MoS_2 was ground with 100 milligrams of CS for a period of 10 minutes. 0.5 mL of IL was then added into the mortar, followed by grinding for another 50 min. The grinding mixture was collected from the mortar and pestle, and then washed with acetone, DMF and 0.5% acetic acid to remove the ionic liquid and the excess chitosan. This washing cycle was repeated three times. Finally, the sediment was dispersed in water and centrifuged at a speed of 1500 rpm for 20 min to remove the large/thick MoS_2. The obtained CS-MoS_2 nanosheets dispersion was diluted with water to 100 mL and stored in 4 ℃ for the following investigations. The concentration of MoS_2 sheets in suspension was determined by atomic absorption spectroscopy (AAS) (Z-2000, Hitachi).[2]

Characterizations

Fourier transform infrared (FT-IR) spectroscopy was recorded on a Vetex70 (BRUKER Corp., Germany). The weight loss curves were obtained with thermo gravimetric analyzer apparatus (STA449F3, Netzsch, Germany) from room temperature to 600 ℃ at the rate of 10 ℃/min in N_2 calcinations. Raman measurements were done using HR LabRam Raman spectroscopy system. The UV-vis spectra were measured with a UV-2550 spectrophotometer (Shimadzu, Japan) at room temperature. Field emission scanning electron microscope (SEM) image was taken by an S-4800 (Hitachi, Japan). Transmission electron microscopy (TEM) measurements were performed with an H-600 (Hitachi, Japan). AFM measurement was performed on a Bruker NanoScope V instrument in tapping mode.

In *vitro* cytotoxicity of CS-MoS_2 nanosheets

The in *vitro* cytotoxicity experiments were carried out using a human hepatocyte carcinoma cell line (HepG2) derived from a well differentiated human hepatoblastoma. HepG2 were cultured in RPMI-1640 medium supplemented with 10% fetal bovine serum (FBS), benzylpenicillin (100 kU/L) and streptomycin (100 mg/L) at 37 ℃ and in atmosphere of 5% CO_2.[46] To determine the cell viability under dark condition (i.e. without laser treatment), HepG2 (2×10^5 cells/well) was seeded into 24 well cell-culture plates and incubated for 24 h at 37 ℃. Then, cells were treated with different concentrations of CS-MoS_2 nanosheets for 24 h. Following treatment, cells were rinsed with DPBS and treated with 50 μL 5 mg/mL MTT reagent in serum-free media. After incubation for further 3 h, formazan crystals in each well were solubilized in 0.5 mL of dimethyl sulfoxide (DMSO). The final solution in each well was centrifuged at 13,000 rpm to remove any solid residues. The optical absorbance at 490 nm was then recorded by a Microplate reader (Thermo Multiskan MK3).

Photothermal activity of CS-MoS_2 nanosheets

As an efficient NIR absorber, the photothermal activity of th as-prepared CS-MoS_2 nanosheets was assessed. Firstly, CS MoS_2 nanosheets dispersion was diluted to vari t concentrations and 5 mL of each solution was taken in a 10 n glass beaker. This solution was then illuminated with an 808 nm NIR laser with a power density of 2 W/cm^2. Light induce heating in the solution was measured at 1 min intervals with a thermometer located inside the suspension for a total time of 2 min.

For NIR photothermal therapy, cells were seeded as previously. 24 h after cell seeding, the medium was replaced with the diluted CS-MoS_2 and incubated for further 24 h. Afte that, cells were washed thoroughly by fresh serum-free medi and exposed to an 808 nm NIR laser source with the bear diameter of about 1 cm and power density of 2 W/cm^2. The cells were incubated for additional 24 h and cell viabilities w measured by MTT assay as previously described. Besides, to have some optical images from the photothermal destruction of the cells, cancer cells that cultured with 50 μg/mL CS-MoS_2 nanosheets were exposed to the NIR laser irradiation for various periods of time. After further incubation for 24 h, cell was washed with PBS and stained with 0.04% trypan blue solution for 10 min. Microscopic images of cells were then taken using a microscope.

Statistical analysis

All data were expressed as mean values ± standard deviation (SD). The intergroup variation was measured by one-way analysis of variance (ANOVA) followed by Duncan's multipl range tests. The level of statistical significance was established at $p < 0.05$.

Conclusions

In this contribution, we have demonstrated an easy way for t one-step exfoliation and functionalization of molybdenum disulfide in ionic liquid using an agate mortar with a pestle only. The concentration of the resulting product was as high as ~0.5 mg/mL accompanied with high-yield approaching 17%. The present exfoliation process establishes a high-throughput and soft method for the top-down fabrication of modified MoS_2 nanosheets, as compared to the conventional approach of using organolithium or various organic solvent with sophisticated equipment. The as-fabricated CS-MoS_2 nanosheets dispersions are endowed with well dispersity in aqueous solution, good biocompatibility for photothermal therapy. The ease of synthesis and functionalization of MoS_2 nanosheets make this inexpensive and rising nanostructure more attractive in the application of nanomedicine.

Acknowledgements

This work is supported by Program for New Century Excellent Talents in University (NCET-13-0483), Open Fund of S

Key Laboratory of Electroanalytical Chemistry (SKLEAC201301) and the Shaanxi Provincial Research Fund (2014KJXX-42, 2014K02-13-03, 2014K13-10).

Notes and references

1 X. Bian, J. Zhu, L. Liao, M. D. Scanlon, P. Ge, C. Ji, H. H. Girault and B. Liu, *Electrochem. Commun.*, 2012, **22**, 128-132.
2 M. D. Quinn, N. H. Ho and S. M. Notley, *ACS Appl. Mater. Interfaces*, 2013, **5**, 12751-12756.
3 L. Liao, J. Zhu, X. Bian, L. Zhu, M. D. Scanlon, H. H. Girault and B. Liu, *Adv. Funct. Mater.*, 2013, **23**, 5326-5333.
4 G. S. Bang, K. W. Nam, J. Y. Kim, J. Shin, J. W. Choi and S.-Y. Choi, *ACS Appl. Mater. Interfaces*, 2014, **6**, 7084-7089.
5 W. Yin, L. Yan, J. Yu, G. Tian, L. Zhou, X. Zheng, X. Zhang, Y. Yong, J. Li and Z. Gu, *ACS nano*, 2014, **8**, 6922-6933.
6 T. Liu, C. Wang, X. Gu, H. Gong, L. Cheng, X. Shi, L. Feng, B. Sun and Z. Liu, *Adv. Mater.*, 2014, **26**, 3433-3440.
7 R. Anbazhagan, H.-J. Wang, H.-C. Tsai and R.-J. Jeng, *RSC Adv.*, 2014, **4**, 42936-42941.
8 Y.-H. Lee, L. Yu, H. Wang, W. Fang, X. Ling, Y. Shi, C.-T. Lin, J.-K. Huang, M.-T. Chang and C.-S. Chang, *Nano Lett.*, 2013, **13**, 1852-1857.
9 M. Osada and T. Sasaki, *Adv. Mater.*, 2012, **24**, 210-228.
10 B. Radisavljevic, A. Radenovic, J. Brivio, V. Giacometti and A. Kis, *Nat. Nanotechnol.*, 2011, **6**, 147-150.
11 Y. Wang, J. Z. Ou, S. Balendhran, A. F. Chrimes, M. Mortazavi, D. D. Yao, M. R. Field, K. Latham, V. Bansal and J. R. Friend, *ACS nano*, 2013, **7**, 10083-10093.
12 P. Joensen, R. Frindt and S. R. Morrison, *Mater. Res. Bull.*, 1986, **21**, 457-461.
13 J. N. Coleman, M. Lotya, A. O'Neill, S. D. Bergin, P. J. King, U. Khan, K. Young, A. Gaucher, S. De and R. J. Smith, *Science*, 2011, **331**, 568-571.
14 Y. Yao, L. Tolentino, Z. Yang, X. Song, W. Zhang, Y. Chen and C. p. Wong, *Adv. Funct. Mater.*, 2013, **23**, 3577-3583.
15 N. Liu, P. Kim, J. H. Kim, J. H. Ye, S. Kim and C. J. Lee, *ACS nano*, 2014, **8**, 6902-6910.
16 Y. Liu, H. Nan, X. Wu, W. Pan, W. Wang, J. Bai, W. Zhao, L. Sun, X. Wang and Z. Ni, *ACS nano*, 2013, **7**, 4202-4209.
17 T. A. Loh and D. H. Chua, *ACS Appl. Mater. Interfaces*, 2014, **6**, 15966-15971.
18 P. Hapiot and C. Lagrost, *Chem. Rev.*, 2008, **108**, 2238-2264.
19 P. Li, K. Pramoda and T.-S. Chung, *Ind. Eng. Chem. Res.*, 2011, **50**, 9344-9353.
20 T. Fukushima, A. Kosaka, Y. Ishimura, T. Yamamoto, T. Takigawa, N. Ishii and T. Aida, *Science*, 2003, **300**, 2072-2074.
21 Z. Jin, J. R. Lomeda, B. K. Price, W. Lu, Y. Zhu and J. M. Tour, *Chem. Mater.*, 2009, **21**, 3045-3047.
22 B. K. Price, J. L. Hudson and J. M. Tour, *J. Am. Chem. Soc.*, 2005, **127**, 14867-14870.
23 N. G. Shang, P. Papakonstantinou, S. Sharma, G. Lubarsky, M. X. Li, D. W. McNeill, A. J. Quinn, W. Z. Zhou and R. Blackley, *Chem. Commun.*, 2012, **48**, 1877-1879.
24 Y. Hernandez, V. Nicolosi, M. Lotya, F. M. Blighe, Z. Sun, S. De, I. McGovern, B. Holland, M. Byrne and Y. K. Gun'Ko, *Nat. Nanotechnol.*, 2008, **3**, 563-568.
25 E. P. Nguyen, B. Carey, T. Daeneke, J. Z. Ou, K. Latham, S. Zhuiykov and K. Kalantar-Zadeh, *Chem. Mater.*, 2015, **27**, 53-59.
26 J. Zheng, H. Zhang, S. Dong, Y. Liu, C. T. Nai, H. S. Shin, H. Y. Jeong, B. Liu and K. P. Loh, *Nat. Commun.*, 2014, **5**, 2995.
27 G. Cunningham, M. Lotya, C. S. Cucinotta, S. Sanvito, S. D. Bergin, R. Menzel, M. S. Shaffer and J. N. Coleman, *ACS Nano*, 2012, **6**, 3468-3480.
28 M. Tariq, M. G. Freire, B. Saramago, J. A. Coutinho, J. N. C. Lopes and L. P. N. Rebelo, *Chem. Soc. Rev.*, 2012, **41**, 829-868.
29 X. Yu, M. S. Prévot and K. Sivula, *Chem. Mater.*, 2014, **26**, 5892-5899.
30 S. S. Chou, M. De, J. Kim, S. Byun, C. Dykstra, J. Yu, J. Huang and V. P. Dravid, *J. Am. Chem. Soc.*, 2013, **135**, 4584-4587.
31 F. Zhang, X. Chen, R. A. Boulos, F. M. Yasin, H. Lu, C. Raston and H. Zhang, *Chem. Commun.*, 2013, **49**, 4845-4847.
32 H. Zhang, K. P. Loh, C. H. Sow, H. Gu, X. Su, C. Huang and Z. K. Chen, *Langmuir*, 2004, **20**, 6914-6920.
33 H. Bao, Y. Pan, Y. Ping, N. G. Sahoo, T. Wu, L. Li, J. Li and L. H. Gan, *Small*, 2011, **7**, 1569-1578.
34 B. L. Li, H. Q. Luo, J. L. Lei and N. B. Li, *RSC Adv.*, 2014, **4**, 24256-24262.
35 E. Varrla, C. Backes, K. R. Paton, A. Harvey, Z. Gholamvand, J. McCauley and J. N. Coleman, *Chem. Mater.*, 2015, **27**, 1129-1139.
36 J. H. Jeon, R. K. Cheedarala, C. D. Kee and I. K. Oh, *Adv. Funct. Mater.*, 2013, **23**, 6007-6018.
37 S. Zhuo, Y. Xu, W. Zhao, J. Zhang and B. Zhang, *Angew. Chem.*, 2013, **125**, 8764-8768.
38 N. A. Travlou, G. Z. Kyzas, N. K. Lazaridis and E. A. Deliyanni, *Langmuir*, 2013, **29**, 1657-1668.
39 S. S. Chou, B. Kaehr, J. Kim, B. M. Foley, M. De, P. E. Hopkins, J. Huang, C. J. Brinker and V. P. Dravid, *Angew. Chem.*, 2013, **125**, 4254-4258.
40 Y. Deng, Z. Luo, N. J. Conrad, H. Liu, Y. Gong, S. Najmaei, P. M. Ajayan, J. Lou, X. Xu and P. D. Ye, *ACS nano*, 2014, **8**, 8292-8299.
41 Z. Chen, Z. Li, J. Wang, E. Ju, L. Zhou, J. Ren and X. Qu, *Adv. Funct. Mater.*, 2014, **24**, 522-529.
42 Q. Tian, M. Tang, Y. Sun, R. Zou, Z. Chen, M. Zhu, S. Yang, J. Wang, J. Wang and J. Hu, *Adv. Mater.*, 2011, **23**, 3542-3547.
43 S. Link, C. Burda, M. Mohamed, B. Nikoobakht and M. El-Sayed, *J. Phys. Chem. A*, 1999, **103**, 1165-1170.
44 E. L. K. Chng, Z. Sofer and M. Pumera, *Nanoscale*, 2014, **6**, 14412-14418.
45 W. Z. Teo, E. L. K. Chng, Z. Sofer and M. Pumera, *Chem. - Eur. J.*, 2014, **20**, 9627-9632.
46 W. Zhang, S. Yu, W. Liu, D. Zhang, W. Zhu, Y. Zhang, W. Wu, L. Zhang and J. Wang, *RSC Adv.*, 2014, **4**, 48765-48769.